Effect of annealing on the mechanical properties and fracture mechanisms of a $Zr_{56.2}Ti_{13.8}Nb_{5.0}Cu_{6.9}Ni_{5.6}Be_{12.5}$ bulk-metallic-glass composite

F. F. Wu,[1] Z. F. Zhang,[1,*] S. X. Mao,[1,2] A. Peker,[3] and J. Eckert[4]

[1]*Shenyang National Laboratory for Materials Science, Institute of Metal Research, The Chinese Academy of Sciences, 72 Wenhua Road, Shenyang 110016, China*

[2]*Department of Mechanical Engineering, University of Pittsburgh, 648 Benedum Hall, Pittsburgh, Pennyslvania 15261, USA*

[3]*Liquidmetal Technologies, Inc., Lake Forest, California 92630, USA*

[4]*Physical Metallurgy Division, Department of Materials and Geo Sciences, Darmstadt University of Technology, Petersenstrasse 23, D-64287 Darmstadt, Germany*

The effect of annealing on the mechanical properties and fracture mechanisms of a $Zr_{56.2}Ti_{13.8}Nb_{5.0}Cu_{6.9}Ni_{5.6}Be_{12.5}$ bulk-metallic-glass (BMG) composite subjected to tension and compression was investigated. When the BMG composite was annealed at high temperature, its mechanical properties changed greatly no matter whether tested under tension or compression. Under tensile loading, the as-cast specimen and the specimen annealed at 573 K failed in a shear mode with certain plasticity, but the specimens annealed at 593 K, 623 K, and 693 K for 1 h are very brittle and always failed in mode *I* fracture. Under compressive loading, however, all specimens failed in a shear mode with a fracture angle smaller than 45° and the corresponding plasticity decreased with increasing the annealing temperature. Therefore, significant asymmetry phenomena between the failure mode, the fracture strength, and the plasticity are found in the BMG composite annealed at different temperatures. Based on the experimental results available, we propose that the ratio of the intrinsic shear strength to the cleavage strength is a substantial parameter controlling not only the strength asymmetry, but also the failure mode and the plastic deformation in the BMG composite.

I. INTRODUCTION

In the past three decades bulk-metallic-glass (BMGs) have intrigued wide interest because of their excellent physical, chemical, and mechanical properties. As far as mechanical properties are concerned, BMGs are characterized by high strength and high elastic strain limit, which renders them potential candidates for use as engineering materials.[1–4] Under unconstrained conditions, however, almost all BMGs confront a fateful problem in that they usually fail by the formation of highly localized shear bands, leading to catastrophic failure without obvious macroscopic plasticity.[5,6] This kind of quasibrittle deformation behavior has seriously limited the application of BMGs as engineering materials. To improve the ductility and overcome the catastrophic failure, the easy propagation of localized shear bands must be constrained. There are generally two methods to achieve it: one is to change the geometry of the BMG specimens or apply the stress state in a softer mode,[5,7–10] the other is to create nanocrystalline BMGs (Refs. 11 and 12) or BMG composites reinforced by ductile metal or refractory ceramic particles.[13–17] Recently, ductile metal reinforced BMG composites were successfully fabricated via a cost effective in situ processing method.[18–21] These BMG composites exhibit large compressive and some tensile plastic strain and strongly improved impact toughness compared to other BMG materials.[22] Multiple shears bands are formed in the BMG matrix so that the catastrophic instability along the localized shear band can be avoided by the ductile metal phases.[14] Bcc-β-Zr-type dendrites reinforced $Zr_{56.2}Ti_{13.8}Nb_{5.0}Cu_{6.9}Ni_{5.6}Be_{12.5}$ is one of the outstanding representatives among these BMG composites. It demonstrates

strongly improved Charpy impact toughness and ductility.[18] These remarkable improvements are explained by the effect of the mechanically soft and ductile secondary phase, which acts stabilizing against shear localization and critical shear band propagation. However, so far there are very limited data to reveal the effect of annealing on the deformation and fracture mechanisms of the $Zr_{56.2}Ti_{13.8}Nb_{5.0}Cu_{6.9}Ni_{5.6}Be_{12.5}$ BMG composite containing ductile dendrites in detail. In this paper, therefore, we systematically investigate the effect of different annealing temperatures on the structure and the mechanical properties of a $Zr_{56.2}Ti_{13.8}Nb_{5.0}Cu_{6.9}Ni_{5.6}Be_{12.5}$ BMG composite under tension and compression loading. In particular, the difference in the fracture modes and deformation mechanisms of this BMG composite induced by different stress modes are discussed.

II. EXPERIMENTAL

Ingots with the composition of $Zr_{56.2}Ti_{13.8}Nb_{5.0}Cu_{6.9}Ni_{5.6}Be_{12.5}$ were provided by LIQUIDMETAL TECHNOLOGIES, INC. The samples were prepared by plasma arc melting a mixture of pure elements in a Ti-gettered argon atmosphere on a water-cooled copper plate. The ingots were then remelted for several times until a homogenous melt was formed. The final ingots had a plate-shape geometry with dimensions of $85 \times 57 \times 2.2$ mm^3 (length, height, and width). The as-cast specimens were sealed in vacuum quartz tubes and annealed at 573 K, 593 K, 623 K, 653 K, and 693 K for 1 h, respectively. Then the quartz tubes were taken out from the furnace and cooled in air down to room temperature.

The microstructures and the phases of the prepared ingots were characterized by using a Cambridge S360 scanning
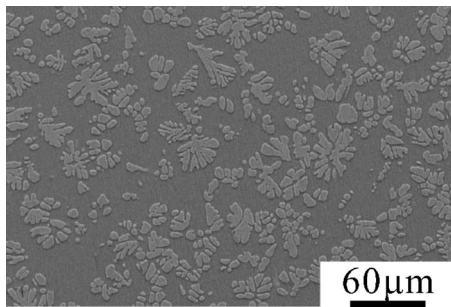
FIG. 1. SEM image of the $Zr_{56.2}Ti_{13.8}Nb_{5.0}Cu_{6.9}Ni_{5.6}Be_{12.5}$ BMG composite etched by Kroll reagent.

electron microscope (SEM), as well as by using a Rigaku x-ray diffractometer (XRD) with Cu $K\alpha$ radiation. Transmission electron microscopy (TEM) was performed using a JEM 2000 FX II electron microscope operated at 200 kV. The sample for TEM was polished mechanically to 25 μm thick, and then thinned by chemical jet technique using a solution of 10% perchloric acid in methanol at a temperature 233 K. The glass transition and the crystallization behavior of the amorphous matrix of the composite were investigated in PERKIN ELMER DSC-7 using a heating rate of 0.167 K/s. Uniaxial tensile and compressive tests were performed on the Zr-based composite specimens with a MTS810 testing machine at room temperature. The tensile specimens were machined into a dog-bone geometry (58 mm overall length with $8 \times 2 \times 2$ mm^3 cross-sectional gauge). The specimens for compression were 4 mm in length with a 2×2 mm^2 rectangular cross section. Two lateral surfaces of each tensile specimen and all lateral surfaces of each compression specimen were polished by 1.5 μm diamond paste. The compression specimens were sandwiched between two tungsten carbide plates in a loading fixture designed to guarantee uniaxial loading. All tensile and compressive tests were conducted using a constant strain rate of about 1×10^{-3} s^{-1}, and were repeated at least 3 times. After the mechanical tests, the specimens were observed by SEM to reveal the deformation and fracture features.

III. RESULTS

A. Microstructure observations

Figure 1 shows the backscattering SEM image of the as-cast BMG composite. The bright phase (25% in volume) corresponds to β-Zr-type dendrites with bcc structure, which are homogeneously dispersed in the gray metallic glass matrix (75% in volume). The compositions of the glass matrix and dendrites are $Zr_{47}Ti_{12.9}Nb_{2.8}Cu_{11}Ni_{19.6}Be_{16.7}$ and $Zr_{71}Ti_{16.3}Nb_{10}Cu_{1.8}Ni_{0.9}$,[18] respectively. The dendritic structure is characterized by primary dendrite axes with a length range of 20–60 μm. Besides, a regular pattern of secondary dendrite arms with a spacing of 2–3 μm is observed. Figure 2 displays a DSC experiment performed with a heating rate of 0.167 K/s, indicating that the glass transition temperature, T_g, is 592 K. Two exothermic peaks are visible during this continuous heating, with the onset of the first peak at 645 K (T_{x1}, the first crystallization starting temperature) and the
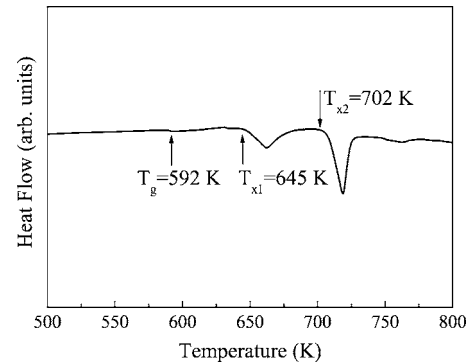

FIG. 2. DSC profiles of the $Zr_{56.2}Ti_{13.8}Nb_{5.0}Cu_{6.9}Ni_{5.6}Be_{12.5}$ BMG composite, performed with a heating rate of 0.167 K/s.

second peak at 702 K (T_{x2}, the second crystallization starting temperature), respectively.

The XRD patterns of the as-cast specimen and of the specimens annealed at different temperatures are presented in Fig. 3. The XRD pattern of the as-cast specimen shows a superposition of a broad diffuse background and a set of specific peaks, which corresponds to a mixture of the metallic glass matrix and the bcc β-Zr solid solution. For the specimens annealed at 573 K and 593 K for 1 h, there is no obvious change in the XRD pattern. But when the specimen was annealed at 623 K for 1 h, there is a slight change in the region near the most intense peak of the bcc β-Zr solid solution. It is believed that the crystallization starts to occur in the metallic glassy matrix because the annealing temperature is very close to the first crystallization starting temperature (T_{X1}=645 K). When annealed at 653 K for 1 h, the specimen displays an obvious new peak to the right of the major peak of the bcc β-Zr solid solution at 2θ=37.9°. The relatively smooth baseline of the diffraction curve indicates a remarkable decrease in the volume fraction of the amorphous phase in the matrix. When annealed at 693 K for 1 h, the specimen undergoes serious crystallization, leading to the appearance of several crystalline peaks besides those of the bcc β-Zr solid solution, which is consistent with the formation of
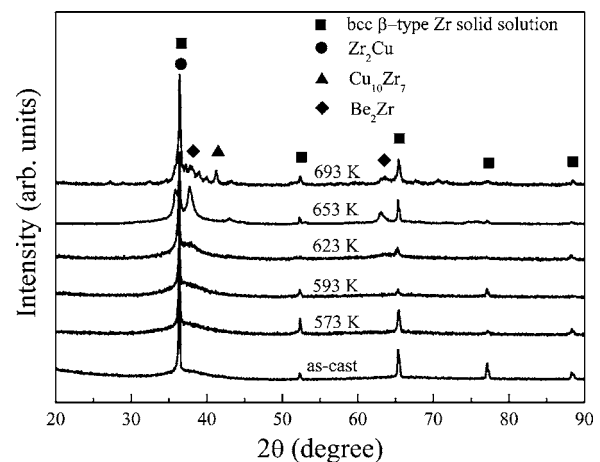

FIG. 3. XRD patterns taken from the as-cast specimen and the specimens annealed at 573 K, 593 K, 623 K, 653 K, and 693 K, respectively.
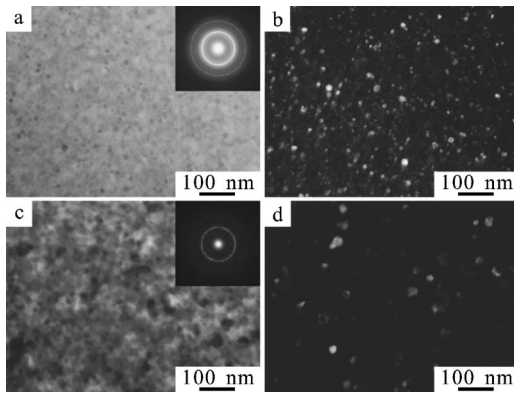
FIG. 4. (a) Bright-field TEM image with diffraction pattern (inset) and (b) dark-field TEM image in the matrix region for the specimen annealed at 653 K; (c) Bright-field TEM image with diffraction pattern (inset) and (d) dark-field TEM image in the matrix region for the specimen annealed at 693 K

$CuZr_2$, ZrCu, and BeZr phases,[23] as marked in Fig. 3. Figure 4 shows the microstructure of the samples annealed at 653 K and 693 K. Both bright-[Figs. 4(a) and 4(c)] and dark-field images [Figs. 4(b) and 4(d)], as well as the diffraction pattern [inset in Fig. 4(a) and 4(c)] clearly show the presence of nanocrystals. The rings in the electron diffraction pattern are relatively well defined; however, they are not solid but dot. The sizes of the nanocrystals are around 20 nm and 35 nm for the specimens annealed at 653 K and 693 K, respectively.

B. Tensile stress-strain curves

Figure 5 shows the tensile true stress-strain curves at a constant strain rate of 1×10^{-3}. The as-cast specimen displays an initial elastic deformation behavior with an elastic strain of about 1.7%, and then begins to yield at about 1402 MPa, followed by a slight strain hardening up to 1475 MPa with a tensile plastic strain of 1.8%. Its tensile fracture stress, σ_F^T, is 1421 MPa. The present results for the as-cast tensile specimen are identical with the previous data reported by Szuecs et al.[19] The specimen annealed at 573 K
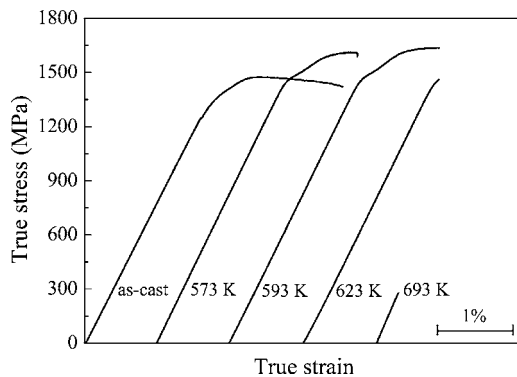

FIG. 5. Tensile true stress-strain curves of the $Zr_{56.2}Ti_{13.8}Nb_{5.0}Cu_{6.9}Ni_{5.6}Be_{12.5}$ BMG composite for (a) the as-cast specimen, and the specimens annealed at (b) 573 K, (c) 593 K, (d) 623 K, and (e) 693 K.
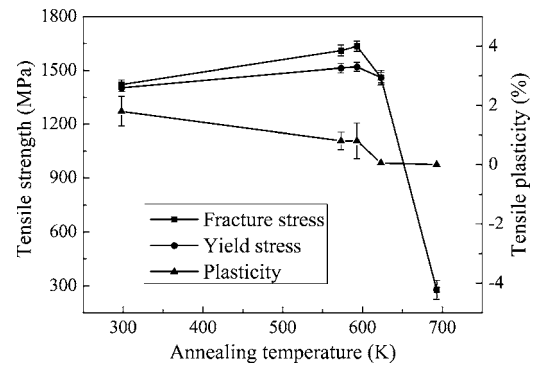

FIG. 6. Dependence of yield strength, fracture strength and plasticity on the annealing temperature of the $Zr_{56.2}Ti_{13.8}Nb_{5.0}Cu_{6.9}Ni_{5.6}Be_{12.5}$ BMG composite.

for 1 h yields at a higher stress of 1513 MPa and deforms continuously until failure at 1611 MPa with a smaller tensile plastic strain of 0.8%. In the case of annealing at 593 K for 1 h, the tensile stress-strain curve does not show obvious difference from that in the case of annealing at 573 K for 1 h. The yield strength, the fracture strength, and the tensile plasticity are 1520 MPa, 1635 MPa, and 0.8%, respectively. However, the specimen annealed at 623 K for 1 h displays a tensile plasticity of only 0.05%, which is far smaller than for the as-cast material and the specimens annealed at 573 K and 593 K for 1 h, respectively, although its fracture strength reaches 1422 MPa. Annealing at 693 K for 1 h leads to zero tensile plasticity with a fracture strength of only 278 MPa, which is the lowest strength among all tested tensile specimens. The dependence of yield strength, fracture strength and plasticity on the annealing temperature is summarized in Fig. 6.

C. Tensile fracture feature observations

SEM observation shows that the fracture under tension always occurs in a shear mode for the as-cast BMG composite, as seen in Fig. 7(a). An obvious necking can be observed, which is consistent with the macroscale tensile plasticity of the specimens. The tensile fracture surface normally makes a shear angle of 54° with the tensile stress axis, which is remarkably larger than 45°. This indicates that the tensile fracture of the composite does not occur along the maximum shear stress plane and thus, accordingly, does not follow the Tresca criterion.[24] Profuse fine slip bands in the dendrites and dense shear bands in the glassy matrix were activated on the specimen surface, which provides evidence for the obvious tensile plasticity, as shown in Fig. 8(a). Due to the constraint of the dendrites, most shear bands were generated from two major directions and then interacted with each other. In contrast, monolithic metallic glasses only display nearly zero plasticity due to a rapid propagation of the major shear band under tension.[5,6] The tensile properties of the current BMG composite are obviously better than those of the Zr-based BMG composites reinforced by tungsten or steel fibers, Ta, WC, or SiC particles under tension.[14,15,25,26] The BMG composite specimen annealed at 573 K for 1 h also failed in a shear mode with a shear angle of 47°, i.e., slightly
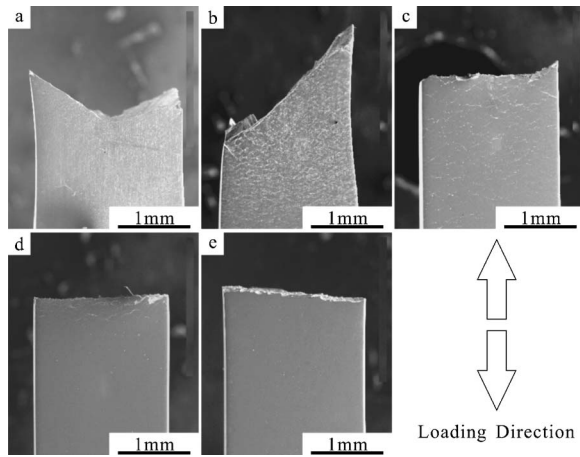
FIG. 7. SEM micrographs showing the macroscopic fracture modes under tensile loading for (a) the as-cast specimen, and the specimens annealed at (b) 573 K, (c) 593 K, (d) 623 K, and (e) 693 K.

larger than 45°, as shown in Fig. 7(b). Its fracture feature is similar to that of the as-cast BMG composite. For the composite specimen annealed at 593 K for 1 h, however, the fracture mode is greatly different from that occurring in the former two specimens. It broke at a fracture angle of nearly 90°, except that a small piece of shear fracture surface occurred near the edge of the specimen, as shown in Fig. 7(c). Further observation [Fig. 8(c)] reveals that there are still some shear bands in the metallic matrix. However, the density of the shear bands is much smaller than for the as-cast specimen or the specimen annealed at 573 K. Most shear bands align along one direction rather than two directions, and no obvious interaction of shear bands can be observed even near the fracture site. Figure 7(d) displays the fracture
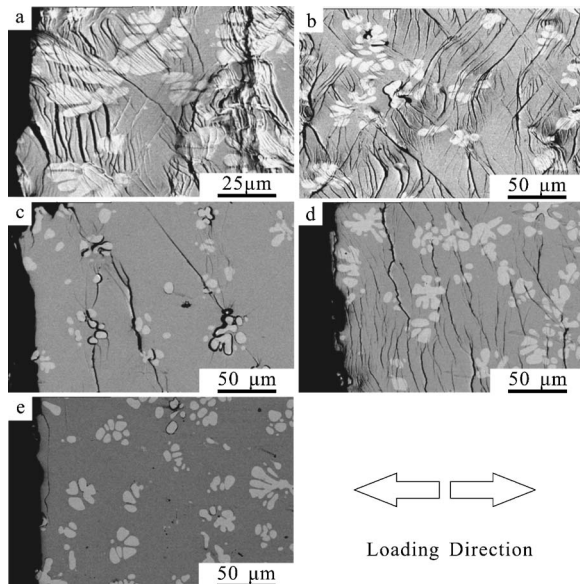

FIG. 8. Backscattering SEM images of the tensile specimens revealing deformation and fracture features for (a) the as-cast specimen, and the specimens annealed at (b) 573 K, (c) 593 K, (d) 623 K, and (e) 693 K.
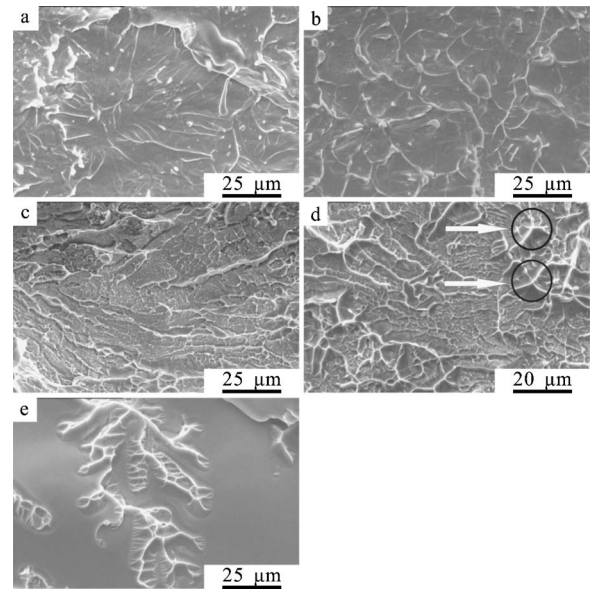

FIG. 9. SEM images showing the fracture surfaces under tensile loading for (a) the as-cast specimen, and the specimens annealed at (b) 573 K, (c) 593 K, (d) 623 K, and (e) 693 K.

of the specimen annealed at 623 K for 1 h. Catastrophic failure occurred at a fracture angle of 90°, which is similar to what was found for the specimen annealed at 593 K. The higher magnified SEM image in Fig. 8(d), however, shows that the density of shear bands is obviously higher than in the case of the specimen annealed at 593 K. Due to the fact that most shear bands are generated from one major direction, the spread of the shear bands is very monotonic, without interaction with each other. For the specimen annealed at 693 K for 1 h, as shown in Fig. 7(e), the tensile fracture also occurs at a fracture angle of 90°, similar as for the specimens annealed at 593 K and 623 K, respectively. Further investigations indicate that only one or two shear bands can be occasionally observed near the fractograph. Also there are no obvious slip bands in the dendrites, which fits in well with the zero tensile plasticity in Fig. 8(e).

The fractographic observations show that for the as-cast specimen and the one annealed at 573 K for 1 h, the typical feature of the fracture surfaces is a veinlike structure, as shown in Figs. 9(a) and 9(b), which is consistent with the observations for fully glassy samples.[5,6] In addition to the veinlike structure, there are many round cores with different diameters on the whole surface. But for the specimens annealed at 593 K and 623 K, the veinlike pattern is very fine and no large melting droplets or round radiating cores can be observed, indicating a slighter remelting during fracture. Furthermore, the broken dendrites are not covered by a fluid layer of the glassy matrix, so that some ridgelike patterns in the dendrites can be seen, as marked in Fig. 9(d). This fracture feature is quite different from those occurring in the as-cast specimen and the specimen annealed at 573 K where the remolten glassy matrix layer covers the fracture surface of the broken dendrites. For the specimen annealed at 693 K, as shown in Fig. 9(e), the fracture surface is characterized by a mixture of very smooth areas in the glassy matrix and some rougher areas in the dendrites, which is characteristic of most
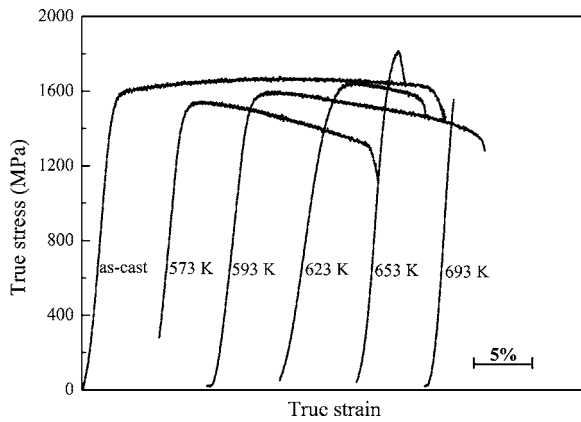
FIG. 10. Compressive true stress-strain curves of the $Zr_{56.2}Ti_{13.8}Nb_{5.0}Cu_{6.9}Ni_{5.6}Be_{12.5}$ BMG composites for (a) the as-cast specimen, and the specimens annealed at (b) 573 K, (c) 593 K, (d) 623 K, (e) 653 K, and (f) 693 K.

ductile fracture surfaces in polycrystalline materials. The predominantly smooth areas are responsible for the catastrophic tensile cleavage failure of this specimen with zero plasticity and low strength (see Figs. 5 and 6).

D. Compressive stress-strain curves

Figure 10 shows the compressive true stress-strain curves at a constant strain rate of 1×10^{-3}, and Fig. 11 presents the dependence of yield strength, fracture strength, and compressive plasticity on annealing temperatures. The as-cast specimen exhibits an elastic strain of about 1.7%, then begins to yield at about 1488 MPa, followed by a slight strain hardening up to 1618 MPa. A compressive plastic strain of 28.3% is achieved before fracture, which is better than the previous result of 5–6% reported by Hays and Szuecs *et al.*[18,19] This should be attributed to its finer spacing of the dendrites, which leads to the formation of finer multiple shear bands. The specimen annealed at 573 K for 1 h yields at 1447 MPa, followed by strain hardening up to 1539 MPa. Then the flow stress decreases continuously until failure at 1316 MPa with a plastic strain of 16.7%. When annealed at 593 K for 1 h,
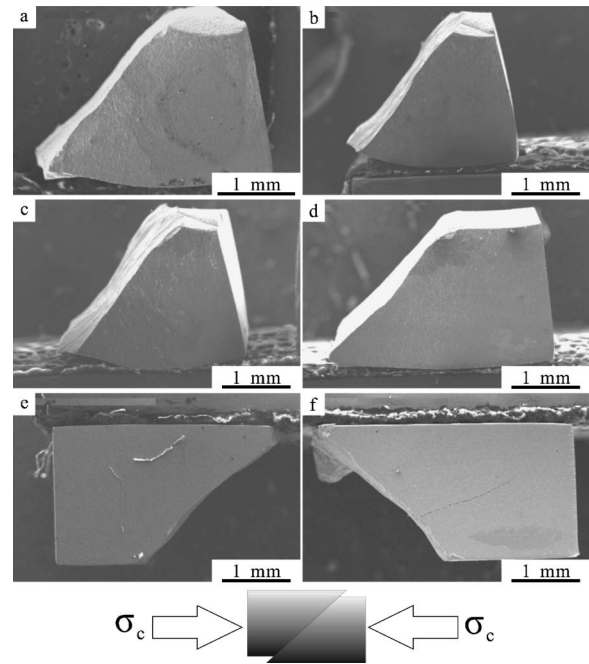
FIG. 12. SEM micrographs of the macroscopic fracture modes under compressive loading for (a) the as-cast specimen, and the specimens annealed at (b) 573 K, (c) 593 K, (d) 623 K, (e) 653 K, and (f) 693 K.

the material has nearly the same stress-strain curve as the specimen annealed at 573 K. Its yield strength, ultimate strength, fracture strength, and plastic strain are 1437 MPa, 1592 MPa, 1350 MPa, and 21.1%, respectively. However, the plastic strain of the specimen annealed at 623 K for 1 h is only 8.7%, which is far smaller than the values of the as-cast specimen and the specimens annealed at 573 K and 593 K. Its ultimate strength and fracture strength are 1640 MPa and 1561 MPa, respectively. When annealed at 653 K for 1 h, the specimen yields at a stress of 1601 MPa, and then fails at 1810 MPa, which is the largest fracture strength among all the tested specimens. The specimen annealed at 693 K for 1 h shows zero tensile plasticity with a fracture strength of 1554 MPa.

E. Compressive fracture feature observations

SEM observation shows that the fracture under compression occurs in a shear mode for the as-cast specimen, as seen in Fig. 12(a). An obvious buckling can also be observed after fracture. The compressive shear fracture surface makes an angle of 40° with respect to the loading axis, which indicates that the shear fracture deviates from the maximum shear stress plane, and also does not follow the Tresca criterion.[24] Dense shear bands in the glassy matrix and slip bands in the dendrites can be clearly observed on the lateral surfaces near the fracture, which contribute to the large plastic strain, as shown in Fig. 13(a). The lateral surface is very rough due to the severe deformation. The specimens annealed at 573 K and 593 K for 1 h also failed in a shear mode with buckling. The shear fracture angles are about 38° and 40°, respectively, as shown in Figs. 12(b) and 12(c). These fracture features are
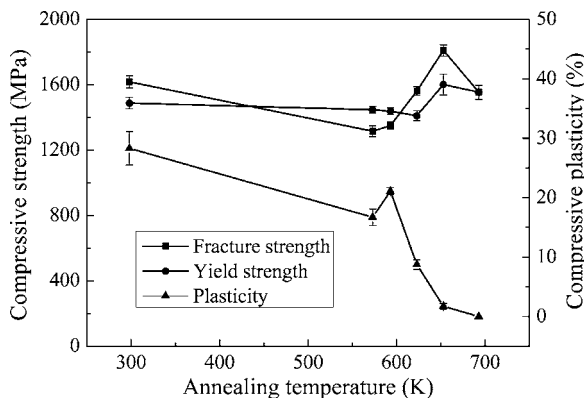

FIG. 11. Dependence of yield strength, fracture strength and plasticity on the annealing temperature of the $Zr_{56.2}Ti_{13.8}Nb_{5.0}Cu_{6.9}Ni_{5.6}Be_{12.5}$ BMG composite.
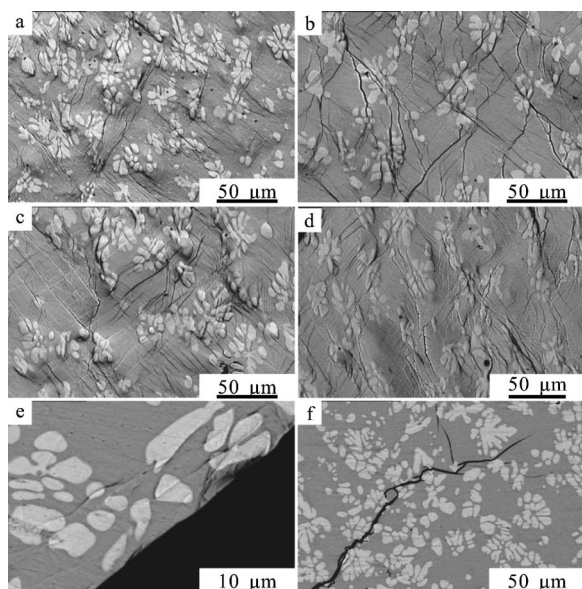
FIG. 13. Backscattering SEM images of the compressive specimen revealing deformation and fracture features for (a) the as-cast specimen, and the specimens annealed at (b) 573 K, (c) 593 K, (d) 623 K, (e) 653 K, and (f) 693 K.
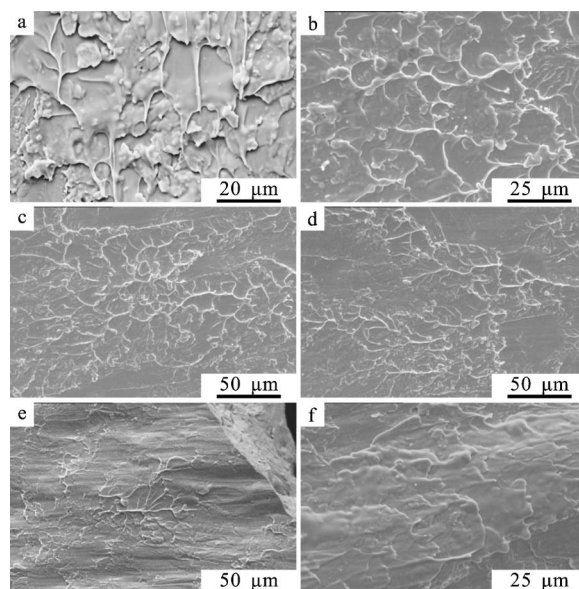

FIG. 14. SEM images showing the fracture surfaces under compressive loading for (a) the as-cast specimen, and the specimens annealed at (b) 573 K, (c) 593 K, (d) 623 K, (e) 653 K, and (f) 693 K.

very similar to that of the as-cast specimen. For the sample annealed at 623 K for 1 h, however, the fracture feature is significantly different from these observations, as shown in Fig. 12(d). Although the samples still fail in a shear mode, there is no buckling such as in the case of the as-cast material. The shear fracture angle is about 37°, i.e., slightly smaller than that of the as-cast one. Further observation [Fig. 13(d)] shows that the density of the shear bands in the glassy matrix is far lower than that for the as-cast one. Figure 12(e) displays the fracture of the specimen annealed at 653 K for 1 h. Its fracture also behaves in a shear mode with a smaller angle of 35°. A higher magnified SEM image shows that only one or two shear bands can be occasionally seen in the vicinity of the fracture surface [Fig. 13(e)]. The direction of the shear bands is more monotonic than that for the as-cast specimen. The limited number of shear bands without interaction with each other leads to the limited compressive plastic strain (1.7%) before fracture. For the specimen annealed at 693 K for 1 h, as shown in Fig. 12(f), the compressive fracture seems to be very similar to the specimen annealed at 653 K. But further investigations revealed that it tends to fail in a split mode and no shear bands can be observed even in the close vicinity of the fracture, as shown in Fig. 13(f). There are also no slip bands occurring in the dendrites. The above observations provide sufficient evidence for the poor compressive plasticity before catastrophic failure of the specimens annealed at 653 K and 693 K (Fig. 10).

The compressive fracture surfaces of the BMG composite are more complex than that of the monolithic metallic glass Vitreloy 1.[5,6] On the fracture surface of the as-cast specimen, there are some areas with vein patterns (in Fig. 14), which is identical with Vitreloy 1.[5,6] Besides, there are some other large areas with rougher surface, which appear to have undergone extensive remelting and resolidification showing certain evidence for enormous heat dissipation during surface separation. With increasing annealing temperature, the extent of remelting and resolidification decreases, as characterized by fewer remelting droplets, fewer veinlike areas, and more smooth areas. However, the fracture surface of the specimen annealed at 693 K shows a special remelting pattern that is much different from all the tested specimens. The whole fracture surface is covered by a special remelted glassy layer, as seen in Fig. 14(f).

IV. DISCUSSION

From the above results, it can be concluded that annealing plays an important role in the mechanical properties and fracture modes for the BMG composite. No matter whether under tension or under compression, the fracture strength, plasticity, and fracture angle always change significantly when the composite is annealed. Upon tensile deformation, the as-cast specimen and the specimen annealed at 573 K fail in a shear mode, but the specimens annealed at 593 K 623 K, and 693 K often display mode *I* fracture.[27] The as-cast specimen has the highest tensile plasticity. The specimens annealed at 573 K and 593 K have a slightly higher fracture strength but relatively low plasticity. However, when annealed at 623 K and 693 K, the specimens have almost zero tensile plasticity.

As far as compressive properties are concerned, the as-cast and annealed specimens also display a similar change as under tension. The as-cast specimen has the best compressive plasticity of 28.3%. When the specimen is annealed at 653 K, the highest strength is achieved, however its plasticity is decreased remarkably to only 1.7%. When annealed at 693 K, the specimen has no plasticity. All the specimens behave in a shear fracture mode with different fracture angles except the specimen annealed at 693 K, that fractures partly
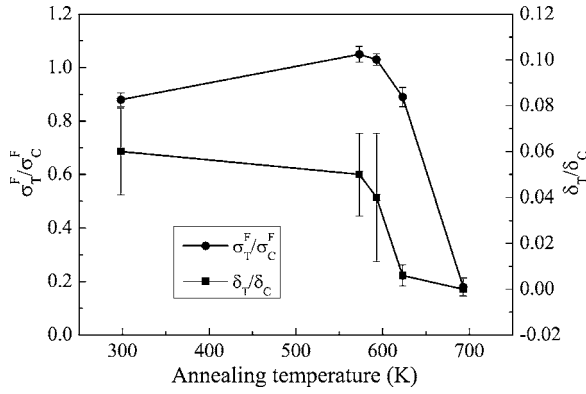
FIG. 15. Effect of the strength and plasticity asymmetries as a fucntion of the annealing temperature.

in a split mode [Fig. 13(f)], which is similar to what was found for BMG composites of $Ti_{50}Cu_{23}Ni_{20}Sn_7$ and $Ti_{56}Cu_{16.8}Ni_{14.4}Sn_{4.8}Ta_8$ that split into several parts or fracture along a plane nearly parallel to the compression axis.[24]

Further analysis shows that there is a pronounced asymmetry between the tensile and the compressive properties of the BMG composite, as summarized in Figs. 15 and 16(a). The as-cast specimen fails in a shear fracture mode with different shear fracture angles ($\theta_T=54°$ and $\theta_C=40°$, respectively) and has an obvious strength asymmetry (σ_T^F/σ_C^F =0.88). However, the tensile and compressive fracture angles of the specimen annealed at 573 K are equal to 47° and 38°, respectively. Moreover, it exhibits a distinctly abnormal
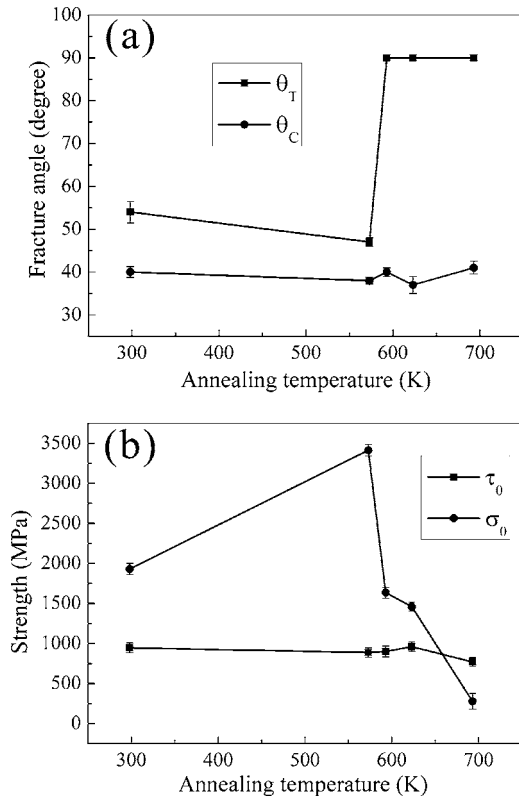

FIG. 16. Effect of (a) fracture angle and (b) shear strength and cleavage strength as a fucntion of the annealing temperature.

strength asymmetry (σ_T^F/σ_C^F=1.05) in comparison with the as-cast specimen. For the specimen annealed at 593 K, the tensile and compressive fracture angles are significantly different, i.e., equal to 90° and 40°, respectively. And it also shows an abnormal strength asymmetry (σ_T^F/σ_C^F=1.03). For the specimen annealed at 623 K, the tensile and compressive fracture angles are 90° and 37°, and the strength asymmetry σ_T^F/σ_C^F is decreased to 0.89. For the specimen annealed at 693 K, the tensile and compressive fracture angles are 90° and 41°, and it displays a remarkable strength asymmetry (σ_T^F/σ_C^F=0.18). Besides, the plasticity before failure is also quite different for the as-cast and the annealed specimens under tension and compression. For example, the tensile plasticity of the as-cast specimen is δ_T=1.8%, but the compressive plasticity δ_C can be as high as 28.3%. So the plasticity asymmetry δ_T/δ_C is 0.06. For the specimen annealed at 573 K, however, the tensile and compressive plasticity are decreased to 0.8% and 16.7%, respectively, resulting in a plasticity asymmetry δ_T/δ_C=0.05. When annealed at 593 K, 623 K, and 693 K, the plasticity asymmetry δ_T/δ_C continuously decreases to 0.04, 0.06, and zero finally. All those data indicate that the Zr-based BMG composite is more sensitive to the stress state (tension or compression) than common metallic polycrystalline materials. Similar phenomena were also widely observed for a variety of materials, such as other BMG materials[24,28–30] or BMG composites,[14,15,25,26,31] graphite, rocks, ceramics, intermetallics, and nanostructured materials.[32–38] This strongly suggests that there must be a common mechanism controlling the deformation and failure of those materials with high asymmetry in strength or plasticity. In the following section, we will elucidate the intrinsic difference in the asymmetries extensively occurring in the Zr-based BMG composite for a better understanding of the strengthening and toughening mechanisms in a variety of materials.

When the as-cast material and the annealed specimens are subjected to tensile loading, they fail either in a normal fracture mode (θ_T=90° for the specimens annealed at 593 K, 623 K, and 693 K) or in a shear fracture mode (θ_T=54° for the as-cast specimen and θ_T=47° for the one annealed at 573 K). To explain the difference in the observed fracture modes, a unified tensile fracture criterion,[39] i.e., ellipse criterion, was proposed

$$(\sigma_n/\sigma_0)^2 + (\tau_n/\tau_0)^2 = 1. \qquad (1)$$

Here, σ_0 is defined as the intrinsic cleavage strength of a material under the condition without shear stress τ_n, and τ_0 is defined as the intrinsic shear strength of a material under the condition without normal stress σ_n. This fracture criterion suggests that the tensile fracture of a material is controlled by both shear and normal stresses (σ_n, τ_n) on the shear plane, and depends on the two intrinsic strengths (σ_0, τ_0). Based on the ellipse criterion above and the tensile Mohr circle, as shown in Fig. 17(a), the tensile fracture angle θ_T can be derived as

$$\theta_T = \frac{\pi}{2} - \frac{1}{2}\arctan\left(\frac{\sqrt{1-2\alpha^2}}{\alpha^2}\right)\ (0 < \alpha = \tau_0/\sigma_0 \leqslant \sqrt{2}/2),$$
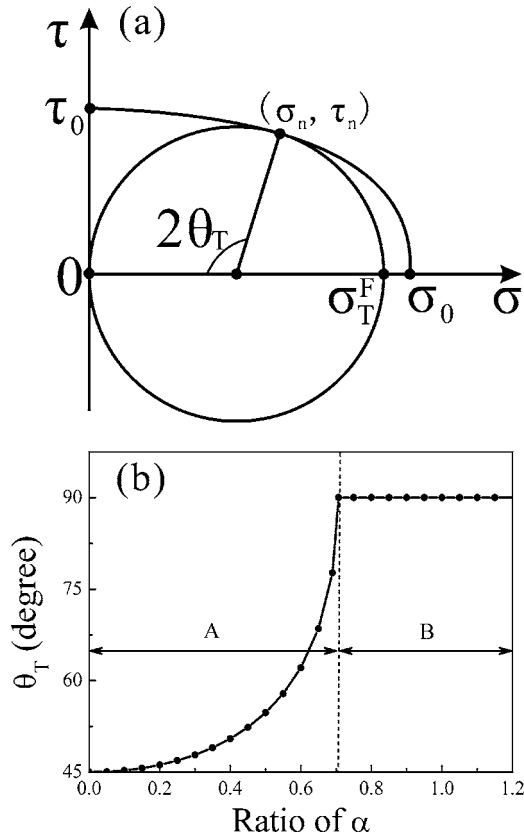
$$(2a)$$

FIG. 17. Illustration of (a) critical tensile failure condition and (b) dependence of tensile fracture angle on the ratio of α according to the ellipse criterion (Ref. 39).

$$\theta_T = 90° \quad (\alpha = \tau_0/\sigma_0 \geq \sqrt{2}/2). \qquad (2b)$$

Here, $\alpha = \tau_0/\sigma_0$ is the ratio of the intrinsic shear strength τ_0 to the cleavage strength σ_0 of a material.[39] Equations (2a) and (2b) reveal that the details of the failure mode of a material, here symbolized as tensile fracture angle θ_T, are strongly controlled by the ratio $\alpha = \tau_0/\sigma_0$. According to Eqs. (2a) and (2b), there are two typical regions marked by A and B, as shown in Fig. 17(b). In region A, the fracture occurs in a shear mode with a shear angle range of 45–90° when the ratio is in the range of $0-\sqrt{2}/2$, which is consistent with the Mohr-Coulomb fracture criterion.[40] Region B corresponds to the mode *I* fracture with a constant angle of 90° when the ratio α is higher than $\sqrt{2}/2$, which is consistent with the maximum normal stress fracture criterion.[40] Due to the difference in the ratio α, the tensile fracture angles θ_T of the BMG specimens distinctly change. Accordingly, the measured tensile fracture angles are 54°, 47°, 90°, 90°, and 90° for the as-cast specimen and the specimens annealed at 573 K, 593 K, 623 K, and 693 K, respectively. Therefore, the ellipse failure criterion can well explain the different tensile fracture modes of the BMG specimens annealed at various temperatures.

According to Eq. (2a), the ratio α can be expressed as

$$\alpha = \tau_0/\sigma_0 = \sqrt{\cos(2\theta_T)/[\cos(2\theta_T) - 1]} \quad (45° < \theta_T < 90°). \qquad (3)$$

Inserting $\theta_T = 54°$ and $\theta_T = 47°$ into Eq. (3), one can derive the ratio $\alpha = 0.49$ and $\alpha = 0.26$ for the as-cast specimen and the specimen annealed at 573 K, respectively. Obviously, the ratio α decreases when the BMG composite is annealed at 573 K.

As is well known, the compressive failure of brittle materials is either controlled by the Tresca criterion or by the Mohr-Coulomb criterion.[24,40–42] For the compressive failure of the Zr-based BMG composites, their shear fracture plane always deviates from the maximum shear stress plane. This indicates that the normal stress must play an important role in the shear fracture processes of BMG composites. Since the fracture stress of these BMG composites is very high, the effect of the normal stress applied on the shear plane should be quite remarkable and will change the critical shear fracture condition of these composites. Normally, it is believed that the deviation of the fracture angle from 45° can be attributed to the effect of normal stress.[40–44] Besides, an obvious asymmetry in the shear fracture of a Zr-based fully glassy alloy was observed under tension and compression due to the different effect of the normal stress on the shear fracture.[30] Hence, the Mohr-Coulomb criterion should be more suitable to describe the critical compression failure condition of the BMG composite, i.e.

$$\tau_n = \tau_0 + \mu\sigma_n, \qquad (4)$$

where τ_n is the critical shear fracture stress, and μ is a constant of the composite. When $\mu = 0$, the Mohr-Coulomb criterion is identical to the Tresca criterion, and the material will fail in a shear mode along the maximum shear stress plane.[40] When $\mu > 0$, the shear fracture of the material will deviate from the maximum shear stress plane. According to the Mohr-Coulomb criterion and the compressive stress Mohr circle, as shown in Fig. 18(a), τ_0 and μ can be calculated as follows:

$$\tau_0 = \sigma_C^F \sin \theta_C (\cos \theta_C + \mu \sin \theta_C), \qquad (5)$$

$$\mu = \frac{\cos(2\theta_C)}{\sin(2\theta_C)} = \text{ctg}(2\theta_C). \qquad (6)$$

From the illustration in Fig. 18(b), it can be seen that the shear fracture angle θ_C strongly depends on the constant μ. Substituting the values of θ_C and σ_C^F from Table I, one can calculate τ_0 and μ for the as-cast composite and the specimens annealed at different temperatures, respectively as listed in Table I. It is apparent that the two constants τ_0 and μ are nearly independent on the annealing temperature, except for the specimen annealed at 693 K. Therefore, all the specimens display approximately the same compressive fracture strength and shear fracture angle.

When the tensile specimens fail in a shear mode, according to Eqs. (3), (5), and (6), the intrinsic cleavage strength σ_0 can be expressed as
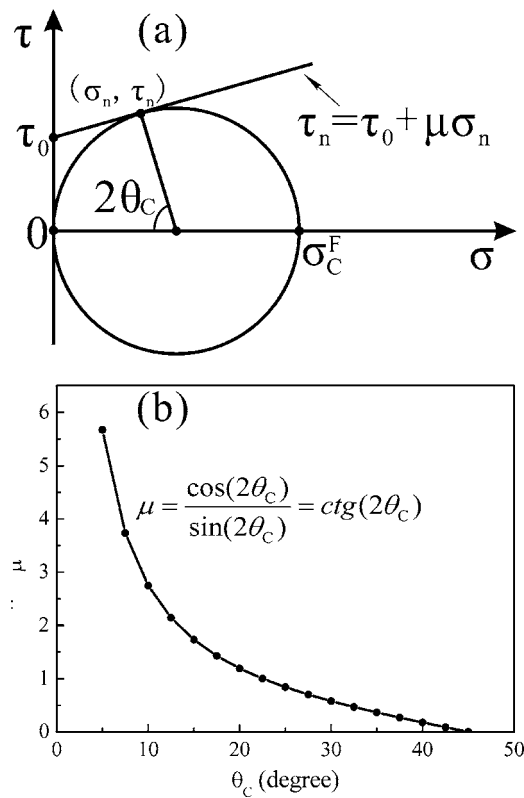
FIG. 18. Illustration of (a) critical compressive fracture condition and (b) dependence of compressive fracture angle on μ according to the Mohr-Coulomb criterion (Refs. 24 and 30).

$$\sigma_0 = \frac{\sigma_C^F \sin\theta_C(\cos\theta_C + \mu\sin\theta_C)}{\sqrt{\cos 2\theta_T/(\cos 2\theta_T - 1)}}. \tag{7}$$

From the data in Table I, one can calculate $\sigma_0 = 1930$ MPa for the as-cast BMG composite and $\sigma_0 = 3412$ MPa for the specimen annealed at 573 K. When the specimens fail in a normal fracture mode, σ_0 is equal to the fracture strength σ_T. Therefore, $\sigma_0 = 1635$ MPa, 1460 MPa, and 278 MPa, respectively, for the specimens annealed at 593 K, 623 K, 693 K. This indicates that the intrinsic strength σ_0 of the BMG composite strongly depends on the annealing temperature, and is significantly improved when the specimen is annealed at

573 K, but is obviously decreased when the specimens were annealed at temperatures above 593 K.

From the above analysis, the measured values of σ_T^F, σ_C^F, θ_C, and θ_T, and the calculated constants τ_0, σ_0, and α are listed in Table I. It can be seen that the ratio $\alpha = \tau_0/\sigma_0$ changes greatly with increasing annealing temperature. For example, the ratio $\alpha = \tau_0/\sigma_0$ of the as-cast specimen is equal to 0.49, which is slightly smaller than the critical value of $\sqrt{2}/2$. Therefore, dense shear bands are easily activated under both tension and compression, resulting in a small strength asymmetry and obvious tensile shear plasticity. In the case of annealing at 573 K, the ratio of $\alpha = \tau_0/\sigma_0$ is equal to 0.26, which is far smaller than the critical value of $\sqrt{2}/2$. Therefore, more shear bands are easily activated under tension and compression, resulting in a smaller strength asymmetry and obvious tensile plasticity. For the specimen annealed at 593 K, the ratio is increased to 0.55, and the activation of shear bands seems to be more difficult than for the specimens annealed at 573 K or without annealing, which leads to a mixed fracture feature with normal and shear modes under tension loading. In the case of annealing at 623 K, the ratio $\alpha = \tau_0/\sigma_0$ is equal to 0.66, which is larger than the former three ratios. Therefore, it is difficult to activate shear bands under tension, which leads to normal fracture under tension and shear fracture under compression. Because no multiple interacting shear bands can be formed under tension, as shown in Fig. 7(d), the tensile plasticity is nearly zero. For the specimen annealed at 693 K, the ratio $\alpha = \tau_0/\sigma_0$ steeply increases to 2.79, which is obviously higher than the critical value of $\sqrt{2}/2$. Hence, shear bands can only be formed under compression, but are absent under tension, as shown in Fig. 7(e). Therefore, mode I fracture (i.e., $\theta_T = 90°$) becomes the preferential failure mode under tension rather than shear deformation for the BMG composite annealed at 693 K, as illustrated in Fig. 16(a). This causes an early normal fracture prior to shear deformation under tension with very low fracture strength ($\sigma_T^F = 278$ MPa) and zero plasticity. Because the tensile fracture strength σ_T^F is controlled by both the intrinsic shear strength τ_0 and the cleavage strength σ_0, it is deduced that the very low tensile fracture strength σ_T^F of the BMG composite annealed at 693 K should be attributed to a large decrease in its cleavage strength σ_0. Therefore, materials with a higher ratio α will exhibit a substantial strength asymmetry under tension and

TABLE I. Mechanical properties and failure modes of $Zr_{56.2}Ti_{13.8}Nb_{5.0}Cu_{6.9}Ni_{5.6}Be_{12.5}$ bulk metallic glass composites containing ductile dendrites. (Note: A=the as-cast specimen, B=the specimen annealed at 573 K, C=the specimen annealed at 593 K, D=the specimen annealed at 623 K, E=the specimen annealed at 693 K.)

| No. | Tension | | | Compression | | | τ_0 (MPa) | σ_0 (MPa) | α | μ | σ_T^F/σ_C^F |
	$\sigma_{T\cdots}^F$ (MPa)	$\delta_{T\cdots}$ (%)	θ_T	$\sigma_{C\cdots}^F$ (MPa)	$\delta_{C\cdots}$ (%)	θ_C					
A	1475±25	1.8±0.5	54°±2.5°	1669±37	28.3±2.8	40°±1.3°	946±60	1930±70	0.49±0.04	0.18	0.88±0.025
B	1611±30	0.8±0.3	47°±1.0°	1539±34	16.7±1.4	38°±0.8°	887±57	3412±74	0.26±0.02	0.24	1.05±0.030
C	1635±28	0.8±0.6	90°	1592±21	21.1±0.6	40°±1.2°	902±68	1635±67	0.55±0.05	0.18	1.03±0.022
D	1460±41	0.05	90°	1640±26	8.7±0.5	37°±1.0°	960±60	1460±55	0.66±0.05	0.29	0.89±0.037
E	278±53	0	90°	1554±43	0	41°±2.5°	769±56	278±59	2.77±0.62	0.14	0.18±0.034

compression. From Fig. 16(b), it is clear that, with increasing annealing temperature, the intrinsic shear strength changes slightly, but the cleavage strength decreases dramatically after annealing at high temperature. Therefore, it is suggested that a high cleavage strength is substantially important to improve the tensile fracture strength.

It is well known that slip and shear deformation are two fundamental modes of plastic deformation for various materials, so materials can slip easily and display great plastic deformation ability, such as fcc single- and poly-crystalline materials.[45] For most BMGs, however, the extremely high compressive fracture strength can be attributed to the great improvement of the intrinsic shear strength τ_0.[39] Also due to the difficulty in the shear deformation, BMGs often exhibit much high fracture strength under tension. But for the fast propagation of a single shear band, BMGs do not exhibit any tensile plasticity.[43,46,47] For the as-cast BMG composite, its shear strength τ_0 and cleavage strength σ_0 match well with the data for monolithic BMGs with a small ratio $\alpha = \tau_0/\sigma_0$,[39] so that the composite deforms and fails in a shear mode. Due to the constraint of the dendrites to the shear bands, multiple shear bands are easily formed displaying certain macroscopic plasticity no matter whether under tension or compression. When annealed at temperatures of 593 K, 623 K, and 693 K, the intrinsic shear strength τ_0 of the BMG composites is hardly changed, but its cleavage strength σ_0 is significantly decreased, leading to a higher ratio $\alpha = \tau_0/\sigma_0$, as shown in Fig. 16(b) and Table I. Therefore, it is hard for the BMG composite to deform in a shear mode and form multiple interacting shear bands. On the contrary, it easily fails in a cleavage mode with zero tensile plasticity and a low farcture strength, as shown in Figs. 7 and 16(a). In this situation, the dendrites have lost their controlling effect to the fast propagation of a single shear band, without formation of multiple shear bands. From the analysis above, it is suggested that the balance (or the ratio $\alpha = \tau_0/\sigma_0$) between the intrinsic shear strength τ_0 and cleavage strength σ_0 is important for the achievement of high tensile properties in BMG materials. Under compression, since the shear deformation often follows the Mohr-Coulomb criterion,[24,30] the BMG materials normally fail in a shear mode. In this case, the multiple interacting shear bands can be activated easily, so the as-cast specimen and the specimens annealed at 573 K, 593 K, 623 K, and 653 K can display certain plasticity to different extent under compression. But the specimens annealed at 693 K show zero plasticity under compression, which can be attributed to the extremely low intrinsic cleavage strength $\sigma_0 = 278$ MPa. As shown in the XRD patterns (Fig. 3), it is quite clear that the phases existed in the BMG composite changed significantly after annealing at different temperatures. Accordingly, it is necessary to further reveal the evolution of the phases and the microstructures during annealing in detail for a better understanding of the relationship between the mechanical properties, failure mechanisms, and the microstructure.

V. CONCLUSIONS

Based on the experimental results and the above analysis, the following conclusions can be drawn:

(1) When subjected to tensile loading, the as-cast $Zr_{56.2}Ti_{13.8}Nb_{5.0}Cu_{6.9}Ni_{5.6}Be_{12.5}$ BMG composite has the best plasticity of 1.8% with a fracture strength of 1475 MPa. With increasing the annealing temperature, the tensile fracture strength increases slightly but the plasticity decreases greatly. After annealing at high temperature, the tensile specimens do not only exhibit zero plasticity, but also display low fracture strength. The as-cast specimen and the specimens annealed at low temperatures fail in a shear mode with different fracture angles under tensile loading. However, the tensile specimens annealed at high temperatures fails in a mode *I* fracture with an angle of 90°.

(2) When subjected to compressive loading, the as-cast $Zr_{56.2}Ti_{13.8}Nb_{5.0}Cu_{6.9}Ni_{5.6}Be_{12.5}$ BMG composite displays the best plasticity of 28.3% with a fracture strength of 1669 MPa. With increasing annealing temperature, the compressive fracture strength changes slightly but the plasticity decreases strongly. When annealed at high temperature, the specimens exhibit almost zero plasticity. All compressive specimens fail in a shear mode with approximately the same shear fracture angles except the specimens annealed at a high temperature of 693 K, which tends to fail in a split fracture mode.

(3) This work shows that both intrinsic shear strength and cleavage strength should be considered when one aims for strengthening a material. It is suggested that the ratio $\alpha = \tau_0/\sigma_0$ plays an important role in the failure modes and the plastic deformation ability under tension for the $Zr_{56.2}Ti_{13.8}Nb_{5.0}Cu_{6.9}Ni_{5.6}Be_{12.5}$ BMG composite. For the as-cast specimen and the specimens annealed at low temperatures, the ratio $\alpha = \tau_0/\sigma_0$ is relatively low, leading to shear fracture and certain plasticity. The tiny or even zero tensile plasticity of the specimens annealed at higher temperatures should be attributed to the obvious increase in the ratio $\alpha = \tau_0/\sigma_0$. It should be significantly important to keep a good balance ($\alpha = \tau_0/\sigma_0$) between the intrinsic shear strength and the cleavage strength to improve the tensile plasticity. This new proposition is of interest for the optimum design of high-performance materials, not only for the new BMG composites but also for nanostructured materials.

*Corresponding author. Email address: zhfzhang@imr.ac.cn

[1] J. F. Loffler, Intermetallics **11**, 529 (2003).

[2] A. Inoue, Acta Mater. **48**, 279 (2000).

[3] W. H. Wang, C. Dong, and C. H. Shek, Mater. Sci. Eng., R. **44**, 45 (2004).

[4] A. I. Salimon, M. F. Ashby, Y. Brechet, and A. L. Greer, Mater. Sci. Eng., A **375**, 385 (2004).

[5] H. A. Bruck, T. Christman, A. J. Rosakis, and W. L. Johnson, Scr. Metall. Mater. **30**, 429 (1994).

[6] H. A. Bruck, A. J. Rosakis, and W. L. Johnson, J. Mater. Res. **11**, 503 (1996).

[7] Y. Yokoyama, K. Yamano, K. Fukaura, H. Sunada, and A. Inoue, Mater. Trans. **42**, 623 (2001).

[8] R. D. Conner, Y. Li, W. D. Nix, and W. L. Johnson, Acta Mater. **52**, 2429 (2004).

[9] Z. F. Zhang, H. Zhang, X. F. Pan, J. Das, and J. Eckert, Philos. Mag. Lett. **85**, 513 (2005).

[10] H. Bei, S. Xie, and E. P. George, Phys. Rev. Lett. **96**, 105503 (2006).

[11] L. Q. Xing, Y. Li, K. T. Ramesh, J. Li, and T. C. Hufnagel, Phys. Rev. B **64**, 180201 (2001).

[12] C. Fan, C. F. Li, A. Inoue, and V. Haas, Phys. Rev. B **61**, R3761 (2000).

[13] H. Choi-Yim and W. L. Johnson, Appl. Phys. Lett. **71**, 3808 (1997).

[14] R. D. Conner, R. B. Dandliker, and W. L. Johnson, Acta Mater. **46**, 6089 (1998).

[15] H. Choi-Yim, R. Busch, U. Köster, and W. L. Johnson, Acta Mater. **47**, 2455 (1999).

[16] W. Zhang, S. Ishihara, and A. Inoue, Mater. Trans. **43**, 1767 (2002).

[17] D. H. Bae, M. H. Lee, D. H. Kim, and D. J. Sordelet, Appl. Phys. Lett. **83**, 2312 (2003).

[18] C. C. Hays, C. P. Kim, and W. L. Johnson, Phys. Rev. Lett. **84**, 2901 (2000).

[19] F. Szuecs, C. P. Kim, and W. L. Johnson, Acta Mater. **49**, 1507 (2001).

[20] G. He, J. Eckert, and W. Loser, Acta Mater. **51**, 1621 (2003).

[21] F. F. Wu, Z. F. Zhang, A. Peker, S. X. Mao, J. Das, and J. Eckert, J. Mater. Res. **21**, 2331 (2006).

[22] G. He, J. Eckert, W. Loser, and L. Schultz, Nat. Mater. **2**, 33 (2003).

[23] X. P. Tang, J. F. Loffler, W. L. Johnson, and Y. Wu, J. Non-Cryst. Solids **317**, 118 (2003).

[24] Z. F. Zhang, G. He, J. Eckert, and L. Schultz, Phys. Rev. Lett. **91**, 045504 (2003).

[25] R. D. Conner, H. Choi-Yim, and W. L. Johnson, J. Mater. Res. **14**, 3292 (1999).

[26] C. Fan, R. T. Ott, and T. C. Hufnagel, Appl. Phys. Lett. **81**, 1020 (2002).

[27] W. D. Callister, *Fundamentals of Materials Science and Engineering* (Wiley, New York, 2001).

[28] G. Wang, J. Shen, J. F. Sun, Z. P. Lu, Z. H. Stachurski, and B. D. Zhou, Intermetallics **13**, 642 (2005).

[29] G. Wang, J. Shen, J. F. Sun, Z. P. Lu, Z. H. Stachurski, and B. D. Zhou, Mater. Sci. Eng., A **398**, 82 (2005).

[30] Z. F. Zhang, J. Eckert, and L. Schultz, Acta Mater. **51**, 1167 (2003).

[31] K. Q. Qiu, A. M. Wang, H. F. Zhang, B. Z. Ding, and Z. Q. Hu, Intermetallics **10**, 1283 (2002).

[32] J. F. Shackelford and W. Alexander, *Mater. Sci. Eng. Handbook* (CRC Press, Florida, 2000).

[33] A. C. Lund and C. A. Schuh, Acta Mater. **53**, 3193 (2005).

[34] S. Cheng, J. A. Spencer, and W. W. Milligan, Acta Mater. **51**, 4505 (2003).

[35] R. Asthana, R. Tiwari, and S. N. Tewari, Mater. Sci. Eng., A **336**, 99 (2002).

[36] T. Engelder, J. Struct. Geol. **21**, 1049 (1999).

[37] M. Radovic, M. W. Barsoum, T. El-Raghy, S. M. Wiederhom, and W. E. Luecke, Acta Mater. **50**, 1297 (2002).

[38] M. Ishihara, J. Sumita, T. Shibata, T. Iyoku, and T. Oku, Nucl. Eng. Des. **233**, 251 (2004).

[39] Z. F. Zhang and J. Eckert, Phys. Rev. Lett. **94**, 094301 (2005).

[40] M. H. Yu, *Unified strength theory and applications* (Springer, Berlin, Germany, 2001).

[41] J. J. Lewandowski and P. Lowhaphandu, Philos. Mag. A **82**, 3427 (2002).

[42] C. A. Schuh and A. C. Lund, Nat. Mater. **2**, 449 (2003).

[43] C. T. Liu *et al.*, Metall. Mater. Trans. A **29**, 1811 (1998).

[44] P. E. Donovan, Acta Metall. **37**, 445 (1989).

[45] C. R. Brooks and A. Choudhury, *Failure analysis of engineering materials* (McGraw Hill, New York, 2001).

[46] C. Fan and A. Inoue, Mater. Trans., JIM **40**, 1376 (1999).

[47] A. Inoue, H. M. Kimura, and T. Zhang, Mater. Sci. Eng., A **294**, 727 (2000).